Food Bioscience 41 (2021) 100929

Contents lists available at ScienceDirect

Food Bioscience

journal homepage: www.elsevier.com/locate/fbio

# Microencapsulation of pomegranate seed oil using a succinylated taro starch: Characterization and bioaccessibility study

M.C. Cortez-Trejo [a], A. Wall-Medrano [b], M. Gaytán-Martínez [a], S. Mendoza [a,*]

[a] Programa de Posgrado en Alimentos del Centro de la República (PROPAC), Research and Graduate Studies in Food Science, School of Chemistry, Universidad Autónoma de Querétaro, 76010, Santiago de Querétaro, Querétaro, Mexico
[b] Instituto de Ciencias Biomédicas. Universidad Autónoma de Ciudad Juárez, 32310, Ciudad Juárez, Chihuahua, Mexico

ARTICLE INFO

*Keywords:*
Pomegranate seed oil
Taro modified starch
Spray drying
Bioaccessibility

ABSTRACT

Pomegranate and taro are domesticated and underutilized crops in Mexico. Particularly, pomegranate seed oil (PSO), which exhibits health benefits, is scarcely exploited in the food industry due to oxidative degradation. This work evaluates the microencapsulation of pomegranate seed oil by spray drying using succinylated taro starch (STS) and β-cyclodextrin (β-CD), as an alternative strategy to protect and deliver PSO. A Central Composite Design (CCD) was applied and the treatment with the highest PSO encapsulation efficiency (61.09 ± 0.41%) was selected. PSO-loaded microparticles obtained with 15% feed solids using 190 °C inlet air temperature, showed low $a_w$ (0.08 ± 0.01), moisture (1.26 ± 0.05%), hygroscopicity (11.69 ± 0.57%), and water solubility (9.81 ± 0.24%). The microencapsulation improved PSO oxidative stability. The *in vitro* bioaccessibility study and the kinetic analysis, on the other hand, evidenced that microparticles of succinylated taro starch obtained by spray drying are suitable as carriers for active compounds to be released at the small intestine following a swelling-controlled release mechanism.

## 1. Introduction

Pomegranate (*Punica granatum* L.) is a fruit-bearing deciduous shrub. Its harvest is widely distributed in the Middle East (Iran, India, China), Mediterranean countries (Spain, Turkey, North Africa), USA, Argentina, and Mexico (Mondragón-Jacobo et al., 2013). The pomegranate fruit is rich in micronutrients and phytochemicals of nutraceutical value. Pomegranate seeds are confined within a juicy sack and they contain 12–20% edible oil rich in punicic acid (18:3: 9-cis,11-trans,13-cis), phytosterols (Bakry et al., 2016; Boroushaki et al., 2016), and phenolic compounds (Boroushaki et al., 2016; Siano et al., 2016). Punic acid is a fatty acid with a powerful antioxidant, anticarcinogenic, immunomodulatory, and lipid metabolism regulator effect. However, due to the reactivity of its conjugated double bonds, punicic acid is chemically unstable and can easily be oxidized, especially when exposed to air, moisture, light, and heat (Siano et al., 2016). Therefore, pomegranate seed oil (PSO) low oxidative stability limits its direct use in food products. In this context, its encapsulation is an alternative to overcome this disadvantage.

The encapsulation process involves the packing of bioactive compounds within structured particles of one or more polymeric materials (wall material) providing them with a stable chemical environment until their release at a desired time and place (Bakry et al., 2016; Veiga et al., 2019). Some essential oils have been microencapsulated using natural biopolymers such as acacia gum, maltodextrins, and modified starches (Bakry et al., 2016; Baranauskienė et al., 2016).

Recently the use of modified starches has gained attention because they are low-cost fat-free ingredients (Altuna et al., 2018; Baranauskienė et al., 2016). Particularly, esterification of native starches with octenyl succinic anhydride (OSA) enhances their hydrophobicity, while maintaining the hydrophilicity of their carbon skeleton (Bhosale & Singhal, 2006). These modified starches are commonly known as "OSA starches" and are effective emulsifiers that can be suitable for the encapsulation of oils. Considering the low viscosity of their aqueous solutions they are also good candidates to form microcapsules using the spray drying technique (Baranauskienė et al., 2016).

Taro (*Colocasia esculenta* L.) on the other hand, is an endemic food crop of Asia and the Pacific islands. This tuber crop is widely cultivated in the United States and some Latin-American countries. Taro tuber is growing in the south of Mexico. However, its consumption is low and limited to the preparation of regional food (Agama-Acevedo et al., 2011). Taro is considered the world's fifth-most extensive root crop

* Corresponding author.
*E-mail address:* smendoza@uaq.mx (S. Mendoza).

https://doi.org/10.1016/j.fbio.2021.100929
Received 12 October 2020; Received in revised form 30 December 2020; Accepted 18 February 2021
Available online 23 February 2021

because of its multipurpose values in food, medicinal, and ornamental aspects. Taro starch is the center of attraction for food researchers and chemical technologists owing to its cheap availability all year long (Singla et al., 2020). It has been succinylated and proposed to be used for encapsulation purposes (Hoyos-Leyva, Bello-Pérez, et al., 2018, b; 2019; Rincón-Aguirre et al., 2018).

PSO has been encapsulated using proteins (Goula & Adamopoulos, 2012), maltodextrin (Goula & Lazarides, 2015), gums (Yekdane & Goli, 2019), and protein-polysaccharide mixtures (Costa et al., 2020; Gupta et al., 2012). Regarding modified starches, PSO has been encapsulated by spray drying using N-LOK starch and whey protein (Sahin-Nadeem & Özen, 2014), corn modified starch Capsul® (Bustamante et al., 2017), and combinations of whey protein with Capsul® (Comunian, da Silva Anthero, et al., 2020, Comunian, Roschel, da Silva Anthero, de Castro, & Hubinger). However, further studies on PSO microencapsulation release and oxidative protection performance are needed. Furthermore, the evaluation of non-conventional starches such as succinylated taro starch as encapsulation material will provide information for the development of novel food products. In this context, this work is aimed to evaluate the potential of succinylated taro starch (STS) to encapsulate PSO using the spray drying technique for PSO oxidative protection and controlled release.

## 2. Materials and methods

### 2.1. Materials

A commercial kit for resistant starch was provided by MEGAZYME® (Megazyme International Ireland Ltd., Wicklow, Ireland). Solvents, either of analytical or HPLC grade, were obtained from Baker (Mallinckrodt Baker, Inc., Phillipsburg, NJ, USA). Enzymes, FAME kit C4–C24-18919, OSA, sodium methoxide ($NaOCH_3$), and all other chemicals were purchased from Sigma (Sigma Aldrich Co., St. Louis, MO, USA).

### 2.2. Extraction and characterization of PSO

Ripen and good quality pomegranates (cv. Apaseo) were obtained from a local producer (Apaseo el Alto, GTO, Mexico). Seeds were separated, washed, dried (45 °C, 24 h), grounded using a coffee grinder, mixed with hexane (1:4 w/v), and sonicated (Branson® 1510R-MTH, Emerson Electric Co., Danbury, CT, USA) for 45 min at room temperature (22–25 °C). The extract was centrifuged at 7620×*g* (9000 rpm in a rotor 221.22 V20, Z326K, Hermle Labortechnik GmbH, Wehingen, Germany) at 4 °C for 10 min and the solvent was removed under vacuum at 40 °C in a rotary evaporator (R-205, BÜCHI Labortechnik AG, Flawil, Switzerland). The remaining extract was set under a nitrogen stream for 3 min and stored at −70 °C.

Identification and quantification of fatty acids in PSO were performed by gas chromatography (Agilent Intuvo 9000 GC System, Agilent Technologies, Palo Alto, CA, USA). Methyl esters of fatty acids were prepared by the sodium methoxide method described by Melo et al. (2016). GC was performed in splitless mode, under the following conditions: injector and detector temperatures of 220 °C and the following temperature gradient: 50 °C for 1 min, 50–220 °C at 25 °C/min, and 220 °C for 32 min. Helium (1 mL/min) was used as the carrier gas. Fatty acids in the samples and punicic acid were identified by comparing their retention times with those of commercial standards (FAME kit C4–C24) and by the reported fragmentation pattern (Lawrence & Brenna, 2006), respectively.

### 2.3. Succinylation of taro starch

Taro was harvested in Jalapa, Tabasco, Mexico. Tubers were washed, cut into 1 cm slices, covered with 1500 ppm sodium sulfite solution, and milled (PULVEX-200, Martillos Pulvex, S.A de C.V., MX, Mexico). The resulting paste was filtered (60 mesh screen) and the residue was washed twice with water. The filtrate was centrifuged at 959×*g* (2500 rpm in a fixed-angle rotor JA-14, Avanti J-301 centrifuge, Beckman Coulter Inc., Palo Alto, CA, USA) at 5 °C for 15 min and the supernatant was discarded. The pellet was washed three times with distilled water. The starch was dried for 16 h at 50 °C and further milled until a 100-mesh powder was obtained. The succinylation of taro starch was achieved by a method previously described (Han & BeMiller, 2007) using some modifications. 200 g of starch were dispersed in 450 mL of water under stirring and the pH was adjusted to 8.5 with 1M NaOH. 2-Octen-1-ylsuccinic anhydride (3.0% of the weight of starch) was added under continuous and vigorous agitation maintaining the pH. After 6 h, the starch slurry was neutralized with 1M HCl and centrifuged at 959×*g* (2500 rpm) at 5 °C for 10 min. The solid was washed three times with water followed by acetone to let it air-dry (50 °C) and milled (100 mesh).

The degree of substitution (DS) of STS was determined following the Bhosale and Singhal (2006) methodology. In this way, a sample (5 g) was dissolved in 50 mL of distilled water and 25 mL of 0.5 M NaOH were added. After 24 h of stirring, this solution was titrated with a 0.05 M NaOH solution using phenolphthalein as indicator. The DS was calculated using Equations (1) and (2) (Viswanathan, 1999):

$$\%\ S = \frac{((B - M)x\ N\ x\ 210.27\ x\ 100\ )/w}{W} \quad (1)$$

$$DS = \frac{162\ x\ S}{21027 - (209\ x\ S)} \quad (2)$$

Where % S is the succinate percentage; B is the titration volume of NaOH solution for the control; M is the titration volume of NaOH solution for the sample; N is the normality of NaOH solution and w is the dry weight of the OSA starch (g). The molecular weights of anhydroglucose (162 g/mol) and OSA (210.27 g/mol) were considered. Resistant starch content (RS) was determined using Megazyme® Resistant Starch Assay Kit following the manufacturer's protocol, and residual protein determination was carried out using the official AOAC (2000) method for protein (46–13) and employing a nitrogen conversion factor of 5.7.

### 2.4. Spray drying

A Central Composite Design (CCD) with a central point of three factors (feed solids concentration, S: 15%, 25%; oil to wall material ratio, r: 1:3, 1:4, and inlet temperature, T: 170 °C, 190 °C. Values based on preliminary studies) was applied using as the response variable the efficiency of encapsulation (EE). The complete design consisted of 15 different combinations (see Table 1). Regression analysis was carried out on the experimental data and the relationship between independent (y) and dependent variables (x), was calculated using a second-order polynomial (see Equation (3)).

$$y = \beta_0 + \beta_1 x_1 + \beta_2 x_2 + \beta_3 x_3 + \beta_{11} x_1^2 + \beta_{22} x_2^2 + \beta_{33} x_3^2 + \beta_{12} x_1 x_2 + \beta_{13} x_1 x_3 + \beta_{23} x_2 x_3 \quad (3)$$

The coefficients of the polynomial equation correspond to: $\beta_0$ for a constant; $\beta_1$, $\beta_2$, and $\beta_3$ for linear effects; $\beta_{11}$, $\beta_{22}$, and $\beta_{33}$ for quadratic effects and $\beta_{12}$, $\beta_{13}$, and $\beta_{23}$ for interaction effects.

Aqueous solutions of STS were prepared at 70 °C and allowed to cool in tap water, then β-cyclodextrin (β-CD) (β-CD/oil molar ratio of 0.071) was added as an aid for emulsification. The β-CD-STS solution was stirred magnetically at room temperature overnight. Then, PSO was emulsified into the hydrated coating material using a homogenizer (Ultra Turrax K10, Wilmington, NC, USA) operating at 20,000 rpm for 9 min. The emulsion (100 mL) was fed to a BÜCHI spray dryer (B-290, Labortechnik AG, Flawil, Switzerland) at room temperature with constant agitation, at a fixed flow rate of 5 mL/min, and using the aspirator

working at 95%. The powder was stored at 4 °C in a sealed amber glass container until analysis.

### 2.5. Surface oil, total oil, and encapsulation efficiency

The surface and total oil in the PSO-loaded microparticles were determined using the methods previously described (Bustamante et al., 2017). For surface oil, 50 mL of hexane was added to 1 g of powder followed by vortexing (30 s). The suspension was filtered (pore size 0.45 μm), the solvent was removed in a rotary evaporator (BÜCHI Labortechnik AG), and the residue was weighed. For total oil, 100 mg of powder were dispersed in 0.25 mL of distilled water. After 20 min 2.5 mL of ethyl acetate, 2.5 mL of ethanol, 2.5 mL of hexane, and 2.5 mL of distilled water were sequentially added to the sample and followed by vortex stirring for 1 min. The organic phase was collected by centrifugation at 1036×*g* (3318 rpm, Hermle Labortechnik GmbH) at room temperature for 5 min. The process was repeated four times. The organic extract was filtered (pore size 0.45 μm), the solvent was removed in a rotary evaporator (BÜCHI Labortechnik AG), and the residue was weighed. The encapsulation efficiency (EE) was calculated using Equation (4).

$$\%\ EE = \frac{(Total\ oil - Surface\ oil)}{Total\ oil} x100 \quad (4)$$

### 2.6. Physicochemical characterization of microparticles

#### 2.6.1. Attenuated total reflectance fourier transform infrared spectroscopy (ATR-FTIR)

IR spectra were obtained with a spectrophotometer (Spectrum GX, PerkinElmer, Waltham, MA, USA) coupled with an ATR accessory. A total of 16 scans were performed and the wavenumber resolution was 4 $cm^{-1}$. Scans were taken over a spectral range of 4000 to 650 $cm^{-1}$.

#### 2.6.2. Morphology, particle size, and bulk density

The morphology of PSO-loaded and unloaded microparticles was studied using SEM (EVO-50, Carl Zeiss, Jena, Germany) operated at 15 kV. The diameters of microparticles were obtained with the public domain software Image J of Java (version 1.8, National Institutes of Health, Bethesda, MD, USA). The number-length mean $D_{(1,0)}$ was calculated measuring 300 microparticles using Equation (5).

$$D_{(1,0)} = \frac{\sum d}{n} \quad (5)$$

Where n is the number of microparticles and d the diameter. The density was determined by transferring 2 g of powder to a container of known volume and weighing (Goula & Adamopoulos, 2012).

#### 2.6.3. Peroxide index (P.I)

To confirm the non-degradation of PSO, the P.I of the microencapsulated oil was evaluated and calculated according to Icyer et al. (2017) with slight modifications. Briefly, 1 g of PSO-loaded microparticles were weighed and transferred into a flask where 6 mL of acetic acid:chloroform solution (3:2 v/v) were added. Then 0.1 mL of saturated KI solution were added, and the mixture was vortexed for 1 min. After keeping the resulting solution in the dark for 10 min, 6 mL of distilled water were added, and titration with 0.002 N sodium thiosulfate ($Na_2S_2O_3$) was performed. The titrating solution was prepared from a $Na_2S_2O_3$ 0.1 N stock solution and standardized with a $K_2Cr_2O_7$ primary standard solution. A potato starch solution 1% w/v was used as indicator and the P.I index was calculated using Equation (6).

$$P.I = (A * N * 1000)/w \quad (6)$$

In this equation, A and N correspond to the volume (mL) and the normality of the $Na_2S_2O_3$ solution, and w is the amount of oil present in the sample (total oil previously calculated). Results were expressed in milliequivalents of active oxygen per kilogram of oil (meq·$O_2$/kg).

#### 2.6.4. Moisture, water activity ($a_w$), solubility in water, and hygroscopicity

The moisture content of PSO-loaded microparticles was determined by drying in a vacuum oven at 105 °C until consecutive weighings, made at 2 h intervals, gave less than 0.3% variation (Goula & Adamopoulos, 2012). The result was expressed in terms of wet basis percentage (kg water/kg wet material × 100). Water activity ($a_w$) on the other hand, was measured with an AquaLab water activity meter (Aqua Lab Series 3 Model TE, Decagon Devices, Inc. Pullman, WA, USA) at 26.8 ± 0.1 °C.

The solubility in water of the samples under study was determined using the method reported by Icyer et al. (2017). A 0.4 g of the sample was mixed with 40 mL of distilled water, homogenized, and vortexed for 1 min. Following the centrifugation of the mixture at 2352×*g* (5000 rpm, Hermle Labortechnik GmbH) at room temperature for 10 min, 20 mL of the supernatant was dried at 70 °C in a vacuum oven for 24 h. The results were expressed as the percentage of solubility on a dry basis.

For the determination of the hygroscopicity, the methodology of Goula and Adamopoulos (2012) was followed applying some modifications. In this way, 0.5 g of powder were sprinkled and distributed in previously weighted Petri dishes. The boxes were placed inside a desiccator at 25 ± 1 °C and 76 ± 2% relative humidity (controlled with supersaturated $Na_2SO_4$ solution) for 90 min. Then, Petri dishes were weighted and the percentage of hygroscopicity was expressed as a percentage of weight gain per gram of powder.

#### 2.6.5. DSC analysis

The thermal properties of PSO-loaded and unloaded microparticles were measured using a differential scanning calorimeter (model Q 2000, TA Instruments, New Castle, DE, USA) using the method previously described (Rincón-Aguirre et al., 2018). Briefly, a 2.3 mg sample were weighed in an aluminum pan and 7.7 μL of deionized water were added. The pan was sealed tightly and then it was allowed to remain for 1 h before conducting the analysis. An empty aluminum pan was used as a reference. The sample was subjected to a heating program over a temperature range from 10 to 120 °C at a heating rate of 10 °C/$min^{-1}$. The glass transition temperature (Tg) and gelatinization temperature or peak temperature (Tp) were obtained from the analysis carried out by the TA Universal Analysis software (TA Instruments, New Castle, DE, USA).

### 2.7. In vitro bioaccessibility

*In vitro* bioaccessibility of microencapsulated PSO was assessed by an *in vitro* gastrointestinal digestion following a modified protocol based on the report of Shen et al. (2011). PSO-unloaded microparticles were used as the blank. *Oral phase*: It was simulated using a salivary fluid donated by healthy individuals in fasting conditions and without brushing their teeth. *Gastric phase*: The simulated gastric fluid (SGF) was prepared on the day of its use. Sodium chloride (20 g) was dissolved in 800 mL of Milli-Q water and adjusted to pH 1.2 using 37% HCl solution. Pepsin 8 U.S.P (3.2 g) was added, and the mixture was stirred for 30 min. The solution was finally made up to 1000 mL with Milli-Q water and stored at 4 °C until required. *Intestinal phase*: The simulated intestinal fluid (SIF) was prepared as follows: 17 g of potassium monobasic phosphate ($KH_2PO_4$) were mixed with 750 mL of Milli-Q water followed by the addition of 192.5 mL of 0.2 M NaOH. The solution was adjusted to pH 6.8 using 1 M NaOH, and 3.15 g of pancreatin were added. The volume of the solution was made up to 1000 mL with Milli-Q water and was stirred overnight at 4 °C. The next day, the solution was equilibrated at room temperature before the addition of bile extract (6.25 g). A solution of $CaCl_2$ was also prepared by dissolving 5.6 g of $CaCl_2$ anhydrous in 1000 mL of deionized water.

For the simulated digestion process, 1 g of microparticles were mixed with salivary fluid (20 mL) and 19 mL of distilled water. The mixture was incubated at 37 ± 0.5 °C for 10 min. Then, 50 mL SGF were added and incubated at the same temperature for 2 h. Aliquots were taken at

30, 60, 90, and 120 min. For simulated intestinal digestion, after incubation of the gastric phase, the mixture was adjusted to pH 6.8 with 1 M NaOH, then, 40 mL of SIF solution were added and further incubated for 20 min. Subsequently, 10 mL of the $CaCl_2$ solution was added. The sample was further incubated for 2 h 40 min. Aliquots were taken at 30, 60, 90, 120, 150, and 180 min. The samples were stored at −70 °C until analysis was carried out.

To evaluate the release behavior of PSO from β-CD-STS based microparticles during *in vitro* gastrointestinal digestion, the PSO released was extracted from the aliquots and then, quantified by a spectrophotometric method using the extract from PSO-unloaded microparticle samples as the blank. For extraction of released oil, 4 mL were taken from aliquots and 4 mL of isopropanol and hexane were added, then the mixture was vortexed for 30 s and centrifuged at 7620×*g* (9000 rpm, Hermle Labortechnik GmbH) at 4 °C for 5 min. The organic phase was collected, another 4 mL of hexane were added, and the previous process was repeated. The total organic phase was filtered (pore size 5 μm) and diluted (1:1000 dilution factor) to read its absorbance in a UV–Vis spectrophotometer (HP 8453, Hewlett-Packard, Palo Alto, CA, USA) at a λ = 272 nm. For the quantification of oil, a calibration curve of PSO was used. Concentrations from 0.01 to 2 mg/mL were prepared. A 1:1000 dilution factor was used to read the absorbance.

Kinetic analysis of PSO release from microparticles was performed by fitting the release profile to mathematical models such as zero (Equation (7)) and first-order decaying (Equation (8)), Peppas (Equation (9)) and Higuchi model (Equation (10)) (Dima et al., 2016):

$$Q(t) = Q_0 + k \cdot t \tag{7}$$

$$^*Q(t) = (1 - e^{-kt})\, Q_\infty \tag{8}$$

$$Q(t) = k \cdot t^n \tag{9}$$

$$Q(t) = k \cdot t^{1/2} \tag{10}$$

In these equations, k is the release rate constant, Q(t) is the cumulative percent of PSO released at time t (for first-order decaying model *Q(t) is the remaining percent of PSO released in the microparticles), t is the time (h), and $Q_0$ is the initial percent of PSO in microparticles ($Q_\infty$ for the first-order model is the limiting percentage of PSO).

### 2.8. Statistical analysis

All measurements were conducted in triplicate and their mean ± standard deviation (SD) values were calculated. The results of the CCD were analyzed by the Response Surface Methodology (RSM) where the second-order polynomial model and the significance of the effects and their interactions were evaluated using analysis of variance ANOVA ($p<0.05$). Statistical analysis of the data was carried out using the JMP 8.0 software package program (SAS Institute Inc., Cary, NC, USA).

## 3. Results and discussion

### 3.1. PSO and STS characterization

The starting material for the spray drying microparticles were obtained from their corresponding natural sources. In this way, pomegranate seed oil was isolated from mature pomegranate with a yield percentage of 15.55 ± 1.06% containing punicic acid (44.4%), oleic acid (11.3%), linoleic acid (10.1%), palmitic acid (6.2%), and stearic acid (4.8%), as the major components; values which are in agreement with some other reports (Amri et al., 2017; Bakry et al., 2016; Boroushaki et al., 2016; Melo et al., 2016). Succinylated taro starch (STS) on the other hand, was obtained with a DS value of 0.022 (succinylation reaction efficiency 93.11 ± 4.53%), 2.1 ± 0.1% of residual protein, and 17.31 ± 2.43% of resistant starch.

### 3.2. Spray drying process

Table 1 summarizes the process conditions and results of product yield, surface oil, total oil, and encapsulation efficiency (EE) for the microparticles obtained from spray drying.

The outlet temperature varied between 99 and 117 °C. Even when this parameter cannot be controlled, it is important for the quality of the final product. High outlet temperatures can generate undesirable changes in the oil (Bakry et al., 2016). On the other hand, spray drying has an advantage, that is, the material is dried in short times which did not affect the quality of the oil, as verified in the P.I determination.

Another important parameter in a spray drying process is the product yield. A 23.1–48.5% range was obtained, oil leakage from microparticles which difficult their flow and promotes accumulation through the drying chamber can be involved.

The EE of PSO loaded β-CD-STS microparticles ranged from 22.81 to 61.09%. The EE highest value was obtained with 15% feed solids concentration, 190 °C inlet air temperature, and 1:3 core to wall material ratio. The EE results are lower than those reported for PSO encapsulated with modified corn starches (68–92%) (Bustamante et al., 2017; Comunian, da Silva Anthero, et al., 2020; Sahin-Nadeem & Özen, 2014). This difference is related to the low DS (0.022) of STS and the absence of protein in the formulation, which is known to improve the emulsifying properties of carbohydrates (Aksoylu & Ergönül, 2017). It is worth mentioning that, even when β-CD was mixed with STS to improve the emulsification process, the quantities used may not be enough. Furthermore, the porous structure of the STS microparticles promotes oil leakage (Hoyos-Leyva et al., 2019). From the regression analysis for the response variable of EE (Table 2), the fitted model was statistically significant ($p<0.01$) with an $R^2$ value of 0.9936, and the non-significant result in the lack-of-fit test revealed its accuracy for the response. The regression equation obtained (Equation (11)) is the following:

$$EE = -5.796x_1 - 0.734x_2 - 1.916x_3 - 1.922x_2^2 - 2.075x_3^2 + 7.583x_1x_2 - 6.732x_2x_3 - 5.951x_1x_3 \tag{11}$$

Where $x_1$ is the feed solids concentration (%), $x_2$ is the core to wall material ratio, and $x_3$ is the inlet temperature (°C).

As the fitted model evidenced, the double effects of the three factors studied as well as the single effect of feed solids concentration had the greatest influence on EE. Fig. 1 shows the effects of the three factors studied on encapsulation efficiency of PSO when one of them was kept constant. It can be observed that when fixing T at 170 °C (Fig. 1A), the EE increases with increasing S and r. However, at T = 190 °C (Fig. 1B), the opposite behavior is observed, the EE increases as S and r decrease. When r = 1:3 (Fig. 1C), the EE increases with decreasing S and increasing T, but at r = 1:4 (Fig. 1D), the EE increases with an increase of S and decreasing T. Finally, for S = 15% (Fig. 1E), EE increases as r decreases and T increases, and at S = 25% (Fig. 1F), EE increases with an increase in r and decrease of T.

On the other hand, for the single effect of feed solids concentration, it was found that the lower the solids content, the higher the encapsulation efficiency (Table 2). Similar behavior has been previously reported for encapsulation by spray drying (Gargurde et al., 2017; Icyer et al., 2017).

From the experimental design, it was not possible to optimize the EE % since a saddle point rather than a maximum value for EE was obtained. Then, the treatment with the highest EE value (treatment 13) was selected for further characterization.

### 3.3. Microparticle characterization

The morphology of β-CD-STS microparticles was evaluated by SEM and as can be seen in Fig. 2, spherical aggregates for both free and PSO loaded microparticles were obtained. The addition of β-CD and PSO do not affect the morphology of STS spray-dried microparticles

**Table 1**
Experimental design and response variables.[a].

| Experimental Run | Conditions | | | | Response variables | | | |
|---|---|---|---|---|---|---|---|---|
| | | | | | Product | Surface oil | Total oil | EE |
| | $X_1$ | $X_2$ | $X_3$ | $X_4$ | yield (%) | (mg/g) | (mg/g) | (%) |
| 1 | 25 | 1:3 | 170 | 103 ± 9 | 30.4 ± 5.5 | 73.7 ± 0.3 | 97.4 ± 1.0 | 24.4 ± 0.5 |
| 2 | 15 | 1:3 | 170 | 102 ± 8 | 44.7 ± 4.3 | 50.3 ± 0.1 | 84.9 ± 0.9 | 40.7 ± 0.8 |
| 3 | 20 | 1:3 | 180 | 111 ± 8 | 34.6 ± 2.3 | 63.8 ± 3.0 | 105.8 ± 2.3 | 39.7 ± 1.5 |
| 4 | 15 | 1:3.5 | 180 | 117 ± 10 | 37.5 ± 0.6 | 54.1 ± 0.1 | 101.6 ± 3.6 | 46.8 ± 2.0 |
| 5 | 20 | 1:4 | 180 | 106 ± 5 | 40.3 ± 0.2 | 46.4 ± 0.2 | 74.8 ± 1.7 | 38.0 ± 1.1 |
| 6 | 25 | 1:4 | 170 | 106 ± 6 | 23.1 ± 1.6 | 59.6 ± 0.9 | 127.3 ± 4.9 | 53.2 ± 1.1 |
| 7 | 20 | 1:3.5 | 170 | 106 ± 9 | 27.6 ± 0.7 | 52.3 ± 0.1 | 89.3 ± 1.5 | 41.5 ± 0.8 |
| 8 | 25 | 1:4 | 190 | 113 ± 1 | 31.2 ± 2.1 | 52.4 ± 3.3 | 67.8 ± 3.9 | 22.8 ± 0.4 |
| 9 | 15 | 1:4 | 190 | 111 ± 6 | 48.5 ± 1.1 | 46.6 ± 1.0 | 69.1 ± 2.0 | 32.6 ± 0.5 |
| 10 | 20 | 1:3.5 | 190 | 115 ± 1 | 36.0 ± 5.2 | 56.4 ± 1.6 | 88.1 ± 1.8 | 36.0 ± 0.6 |
| 11 | 20 | 1:3.5 | 180 | 110 ± 4 | 32.6 ± 3.7 | 43.7 ± 1.1 | 74.1 ± 0.6 | 41.0 ± 2.0 |
| 12 | 25 | 1:3 | 190 | 116 ± 1 | 25.9 ± 1.0 | 53.3 ± 3.4 | 70.1 ± 3.5 | 24.1 ± 1.1 |
| 13 | 15 | 1:3 | 190 | 112 ± 0 | 36.1 ± 3.9 | 41.3 ± 0.5 | 106.1 ± 2.3 | 61.1 ± 0.4 |
| 14 | 15 | 1:4 | 170 | 99 ± 4 | 47.8 ± 0.3 | 51.7 ± 1.1 | 80.8 ± 2.8 | 36.0 ± 0.8 |
| 15 | 25 | 1:3.5 | 180 | 111 ± 0 | 27.6 ± 0.2 | 66.3 ± 1.2 | 101.8 ± 4.5 | 34.8 ± 1.2 |

[a] Central composite design (CCD): Feed solids concentration ($X_1$; %), core to wall material ratio ($X_2$), inlet temperature ($X_3$, °C), outlet temperature ($X_4$, °C), encapsulation efficiency (EE, %). Results are expressed as mean ± SD (n = 3).

**Table 2**
Variance analysis and model fitting for encapsulation efficiency of PSO.

| Analysis of variance and lack-of-fit test | | | | | | |
|---|---|---|---|---|---|---|
| Source | Degree of freedom | Sum of squares | Mean square | F ratio | Prob>F | Significant |
| Model | 29 | 3076.3741 | 339.8020 | 204.9080 | <0.0001 | ** |
| Lack of fit | 20 | 33.0052 | 3.9916 | 2.0593 | 0.1279 | |
| $R^2 = 0.9936$ | | | | | | |

| Parameter estimates | | | | | |
|---|---|---|---|---|---|
| *Term*[a] | *Estimate* | *Std error* | *t ratio* | *Prob>\|t\|* | *Singnificant* |
| $x_1x_2$ | 7.58625 | 0.321156 | 23.62 | <0.0001 | ** |
| $x_2x_3$ | −6.7325 | 0.321156 | −20.96 | <0.0001 | ** |
| $x_1$ | −5.796 | 0.287251 | −20.18 | <0.0001 | ** |
| $x_1x_3$ | −5.95125 | 0.321156 | −18.53 | <0.0001 | ** |
| $x_3$ | −1.9165 | 0.287251 | −6.67 | <0.0001 | ** |
| $x_3x_3$ | −2.074722 | 0.566467 | −3.66 | 0.0015 | ** |
| $x_2x_2$ | −1.922222 | 0.566467 | −3.39 | 0.0029 | ** |
| $x_2$ | −0.734 | 0.287251 | −2.56 | 0.0189 | * |
| $x_1x_1$ | 0.0027778 | 0.566467 | 0.00 | 0.9961 | |

[a] Feed solids concentration ($x_1$; %), core to wall material ratio ($x_2$), inlet temperature ($x_3$,°C). *p<0.05, **p<0.01.

(Gonzalez-Soto et al., 2011; Hoyos-Leyva, Bello-Pérez, et al., 2018, b; 2019, Phunpee et al., 2017). The residual protein in STS (2.1 ± 0.1%), as well as the STS amphiphilic properties, contribute to the aggregate's formation (Gu et al., 2015; Sweedman et al., 2013). Particle size is one of the most important characteristics of biopolymer-based delivery systems, typically particles in the range 50–100 μm are detected by the consumer as individual entities that give a gritty feel (Joye & McClements, 2014). Interestingly, PSO loaded microparticles exhibited a smaller mean diameter (10.16 ± 3.36 μm) than unloaded ones (12.64 ± 2.67 μm) which can be related to the difference in the STS concentration as well as in the cohesive forces between STS and PSO (Beirão-da-Costa et al., 2011). As far as size distribution, diameters of 7–9 μm and 10–12 μm predominates for PSO-loaded and unloaded microparticles, respectively.

To determine intermolecular interactions between PSO and β-CD-STS, the ATR-FTIR spectra of PSO, PSO-unloaded, and loaded microparticles were obtained (Fig. 3). PSO shows the punicic acid characteristic bands at 987 and 936 $cm^{-1}$, which belong to the fingerprint region of punicic acid double bonds. Other bands were observed such as weak absorption bands at 1419 and 759 $cm^{-1}$, which are attributed to the bending/rocking and out-of-plane C–H vibration of cis olefin; the band at 723 $cm^{-1}$ that is assigned to the vibration outside the plane of the C–H bond that corresponds to unconjugated olefins; the faint absorption band at 966 $cm^{-1}$ that corresponds to the isolated trans double bonds; the 3016 $cm^{-1}$ band corresponding to the cis double bond stretching (Siano et al., 2016), and the 1742 $cm^{-1}$ band that is attributed to the ester carbonyl functional group of glycerol and punicic acid (Cao et al., 2014). PSO-unloaded microparticles exhibited the characteristic bands for carbohydrates, bands at 3000-3800 $cm^{-1}$ assigned to the vibrations of hydroxyl groups (O–H) and stretching of the H–C–H bond, bands at 2927 $cm^{-1}$ or 2934 $cm^{-1}$ for C–H stretching associated with anhydroglucose, the band close to 850 $cm^{-1}$ corresponding to the C–H deformations, and two other characteristic bands, 1153 and 924 $cm^{-1}$ attributed to the stretching of the C–O bond (Jiang et al., 2016). The C–O and C–C vibrations from the octenyl succinic group were observed at 1723 and 1569 $cm^{-1}$, respectively (Gu et al., 2015; Jiang et al., 2016; Sit et al., 2013). PSO-loaded microparticles showed bands resulting from the overlapping of STS, β-CD and PSO signals. Due to this high overlapping effect, no band displacement could be observed, then the intermolecular interactions could not be determined.

To establish the use of the PSO-β-CD-STS microparticles in the food industry, density, peroxide index, moisture, water activity ($a_w$), solubility in water, hygroscopicity, and thermic properties were determined as described in the experimental section.

The density of PSO loaded microparticles was 230 ± 37 $kg/m^3$, being lower than the reported value for PSO microparticles of whey protein and carbohydrate mixtures (262–522 $kg/m^3$) (Sahin-Nadeem & Özen, 2014), defatted milk powder (300–600 $kg/m^3$) (Goula & Adamopoulos,

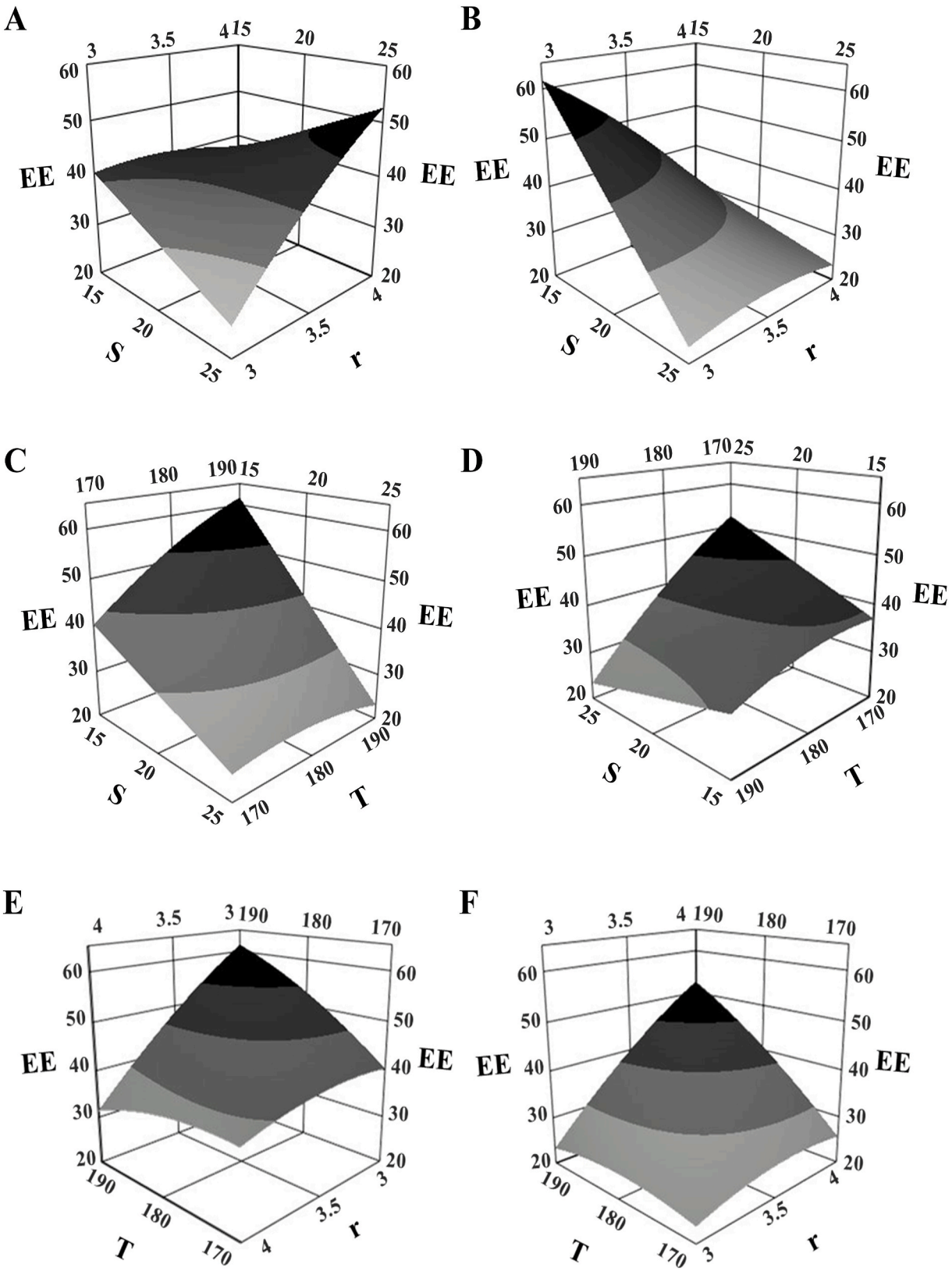


**Fig. 1.** Effect of feed solids concentration (S,%), core to wall material ratio (r), and inlet air temperature (T,°C) (A. At constant T = 170 °C. B. At constant T = 190 °C. C. At constant r = 3. D. At constant r = 4. E. At constant S = 15%. F. At constant S = 25%.) on encapsulation efficiency of PSO.

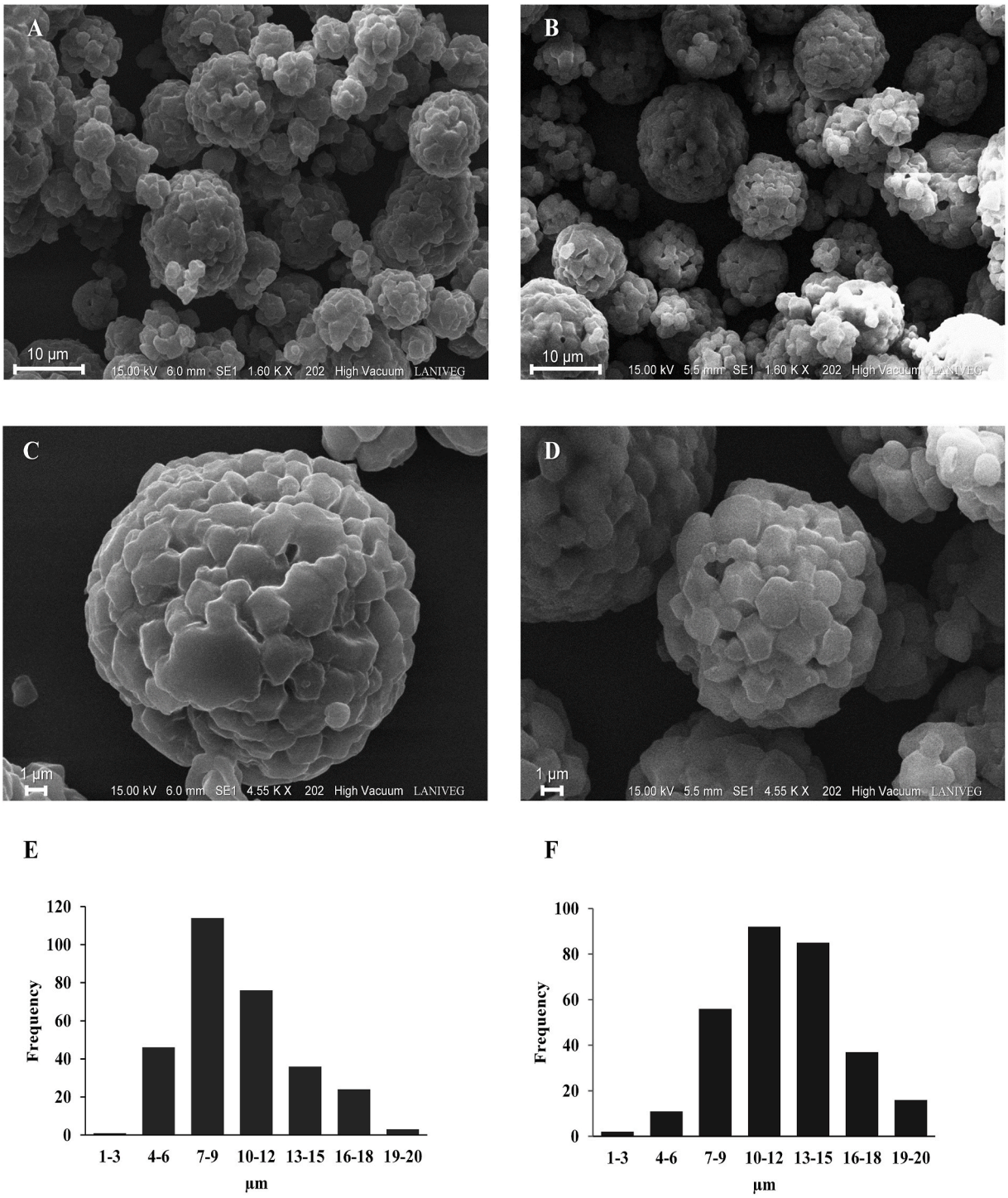


**Fig. 2.** SEM micrographs and size distribution of PSO loaded (A, C, E) and unloaded (B, D, F) microparticles. 1600 X (A, B), 4550 X (C, D).

2012), and whey protein and Capsul® (308 kg/m$^3$) (Comunian, da Silva Anthero, et al., 2020). The different starch source, as well as the morphology of the aggregates (where there is free volume due to the irregular and polyhedral aggregates), affects the bulk density.

According to the Codex Alimentarius (2017) (CODEX-STAN, 210–1999), the lipid oxidation indicator (P.I.) for edible vegetable oils should not exceed 15 meq·$O_2$/kg. Although, some authors suggest values ≥9 meq·$O_2$/kg (Amri et al., 2017). P.I values for PSO before and after spray drying were 2.42 ± 0.03 and 6.20 ± 0.20 meq·$O_2$/kg, respectively. Lipid oxidation of PSO is produced during spray drying. However, P.I. values are acceptable, then, the mixture of STS and β-CD protected oil against heat-induced changes.

The moisture content and $a_w$ of PSO loaded microparticles were 1.26 ± 0.05 and 0.08 ± 0.01%, respectively, and the values were lower than those reported for other PSO microencapsulation systems (Bustamante et al., 2017; Comunian et al., 2020). The differences are mainly attributed to the inlet temperatures used during spray drying, the higher the inlet temperature in the dryer, the higher the exit temperature of the microencapsulated product, and the smaller the moisture content (Veiga et al., 2019). It has been established that lipid oxidation remains at a minimum level within a range of $a_w$ values from 0.20 to 0.40 (Aberkane et al., 2014; Aksoylu & Ergönül, 2017). Considering the low value of $a_w$,

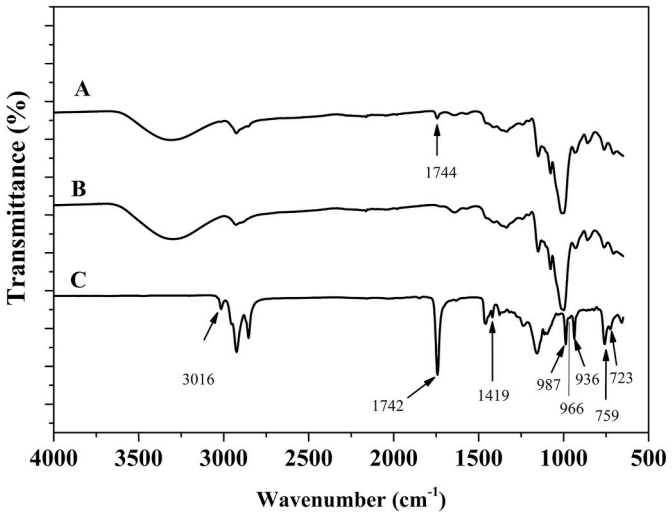


**Fig. 3.** Attenuated Total Reflection-Fourier transforms infrared (ATR-FTIR) spectroscopy. PSO- (C) loaded (A) and unloaded (B) microparticles. Characteristic signals ($cm^{-1}$): *Cis* (3016) and *trans* (966) double bonds, stretching ester bond (1742, 1744), bending/rocking (1419) and out-of-plane (759) C–H vibration of *cis*-olefin, out-of-plane C–H vibration (723) of unconjugated olefins, geometry of double bonds of punicic acid (987, 936).

it is necessary to assess the quality of the microencapsulated oil over time.

For solubility and hygroscopicity, values of 9.81 ± 0.24% and 11.69 ± 0.57% were obtained, respectively. The solubility in water of microparticles determines the type of food matrices where it can be added while hydrophobicity influences storage conditions owing to its relationship with lipidic oxidation. The hydrophobicity of STS prevented higher solubility and hygroscopicity, which is an advantage for handling and storage. On the other hand, the results indicate the PSO-loaded microparticles will be more suitable for food matrices of low water content or oily nature.

Fig. 4 shows the thermal profile of the PSO-loaded and unloaded microparticles under excess of water. The Tg value obtained for PSO-unloaded microparticles was 73.43 °C while a slight decrease is observed for PSO loaded microparticles (72.89 °C) indicating that the addition of PSO increases disorganization of the microparticle structure.

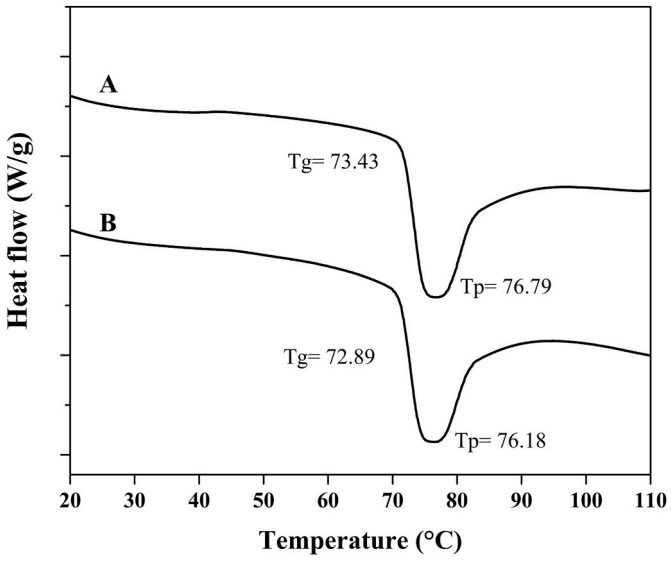


**Fig. 4.** Thermal profiles of PSO-loaded (b) and unloaded (a) microparticles.

### 3.4. In vitro bioaccessibility

In vitro digestion models that simulate physiological gastrointestinal conditions are commonly used to evaluate the extent to which a food component is released from its matrix. Here, the assay was performed to get insight into the gastrointestinal tract fate of the encapsulated PSO.

Fig. 5 shows the cumulative percentage of PSO release from microparticles under *in vitro* gastrointestinal conditions. From this data, under gastric conditions 6.63 ± 0.51% release of PSO was obtained and after intestinal conditions, a maximum of 49.8 ± 1.16% release of PSO was reached. Succinylation besides the spray drying process decreased the digestibility of taro starch (Vernon-Carter et al., 2019; Viswanathan, 1999) by diminishing both the acid and gastric enzymatic degradation of the starch backbone. Moreover, β-CD is poorly digested in the small intestine (Flourié et al., 1993). Then, β-CD-STS microcapsules protect PSO from passage through the stomach, increasing its bioaccessibility in the small intestine. Similar release behavior was reported for linoleic acid microencapsulated with a mixture of xanthan gum/succinylated corn starch, for which 6% and 50.1% release values were observed in the gastric and intestinal phase, respectively (He et al., 2016). It should be noted, that although the bioaccessibility was enhanced in the intestinal phase, the total release of PSO was not reached, which may be a disadvantage. Further studies are required to determine the release behavior in the colonic phase.

The release kinetic analysis of the PSO from β-CD-STS microparticles (Fig. 5) revealed that the Peppas model ($R^2$ = 0.9843) and zero-order model ($R^2$ = 0.9683) describe the transport mechanism of PSO from the β-CD-STS spherical aggregates for gastric and intestinal phase, respectively. From the Peppas model, a diffusion coefficient (n) value n>0.85 was obtained which is related to zero-order release kinetics (case II transport) (Siepmann & Peppas, 2012).

Zero-order release kinetic indicates a swelling-controlled PSO release dominant mechanism, where the microparticles do not disaggregate and the PSO releases very slowly. Then, the swelling process of the β-CD-STS-spherical aggregates that occur during hydration is the rate-controlling step (Siepmann & Peppas, 2012). In this way, water would act as a plasticizer decreasing the glass transition temperature of STS promoting the conversion of glassy to the rubbery state, suggesting that the mobility of the macromolecules and the expansion volume are enhanced when the PSO is released.

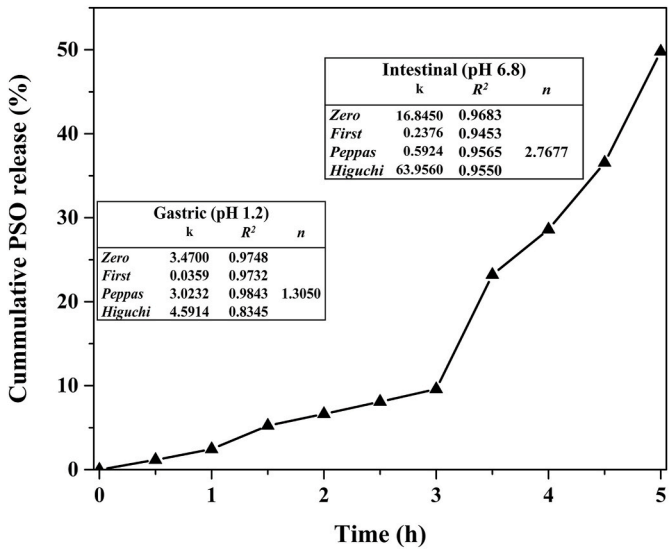


**Fig. 5.** *In vitro* gastrointestinal release profile of PSO and kinetics rate constants and correlation coefficients ($R^2$) by fitting data to several models. Pomegranate seed oil (PSO) released at simulated gastric (pH = 1.2, 2 h, 37 °C) and small intestinal (pH = 6.8, 3 h, 37 °C) conditions.

## 4. Conclusions

β-CD-Succinylated taro starch-based microparticles obtained by spray drying showed potential for a viable and competitive delivery system of lipophilic substances. The PSO loaded microparticles showed low solubility in water, water content, $a_w$, and hygroscopicity which facilitate its handling and storage and its incorporation in predominant oil phase dietary matrices. PSO loaded microparticles were obtained by spray drying process without critically affecting the P.I value of the PSO. However, low EE and high surface oil were obtained. The β-CD-STS microparticle is an encapsulation system to deliver a significant amount of PSO in the small intestine. Further studies are necessary to determine the release behavior of the remaining oil in the colon phase. Additionally, it will be important to study the stability of the microparticles over time.

## CRediT authorship contribution statement

**M.C. Cortez-Trejo:** Conceptualization, Methodology, Validation, Writing – original draft, preparation. **A. Wall-Medrano:** Methodology, Validation, Writing – review & editing. **M. Gaytán-Martínez:** Methodology, Investigation, Writing – review & editing. **S. Mendoza:** Conceptualization, Methodology, Formal analysis, Investigation, Resources, Writing – review & editing.

## Declaration of competing interest

The authors declare no conflict of interest.

## Acknowledgments

The authors would like to thank the National Council of Science and Technology (CONACyT) for the financial support granted through the basic science project CB-2015-1/254063 and UAQ-FOVIN 2018 project 19.

## References

Aberkane, L., Roudaut, G., & Saurel, R. (2014). Encapsulation and oxidative stability of PUFA-rich oil microencapsulated by spray drying using pea protein and pectin. *Food and Bioprocess Technology, 7*(5), 1505–1517. https://doi.org/10.1007/s11947-013-1202-9

Agama-Acevedo, E., Garcia-Suarez, F. J., Gutierrez-Meraz, F., Sanchez-Rivera, M. M., San Martin, E., & Bello-Pérez, L. A. (2011). Isolation and partial characterization of Mexican taro (*Colocasia esculenta* L.) starch. *Starch - Stärke, 63*(3), 139–146. https://doi.org/10.1002/star.201000113

Aksoylu, Z., & Ergönül, G. (2017). A review on encapsulation of oils. *Celal Bayar Üniversitesi Fen Bilimleri Dergisi, 13*(2), 293–309. https://doi.org/10.18466/cbayarfbe.313358

Alimentarius, C. (2017). Codex standard for named vegetable oils Codex stan 210-1999. Codex Alimentarius. Retrieved from http://www.codexalimentarius.org.

Altuna, L., Herrera, M. L., & Foresti, M. L. (2018). Synthesis and characterization of octenyl succinic anhydride modified starches for food applications. A review of recent literature. *Food Hydrocolloids, 80*, 97–110. https://doi.org/10.1016/j.foodhyd.2018.01.032

Amri, Z., Lazreg-Aref, H., Mekni, M., El-Gharbi, S., Dabbaghi, O., Mechri, B., & Hammami, M. (2017). Oil characterization and lipids class composition of pomegranate seeds. *BioMed Research International, 2017*, 1–8. https://doi.org/10.1155/2017/2037341

Aoac. (2000). *Official methods of analysis* (17th ed.). Washington, DC: Association of Official Analytical Chemists.

Bakry, A. M., Abbas, S., Ali, B., Majeed, H., Abouelwafa, M. Y., Mousa, A., & Liang, L. (2016). Microencapsulation of oils: A comprehensive review of benefits, techniques, and applications. *Comprehensive Reviews in Food Science and Food Safety, 15*(1), 143–182. https://doi.org/10.1111/1541-4337.12179

Baranauskienė, R., Rutkaitė, R., Pečiulytė, L., Kazernavičiūtė, R., & Venskutonis, P. R. (2016). Preparation and characterization of single and dual propylene oxide and octenyl succinic anhydride modified starch carriers for the microencapsulation of essential oils. *Food & Function, 7*(8), 3555–3565. https://doi.org/10.1039/C6FO00775A

Beirão-da-Costa, S., Duarte, C., Moldão-Martins, M., & Beirão-da-Costa, M. L. (2011). Physical characterization of rice starch spherical aggregates produced by spray-drying. *Journal of Food Engineering, 104*(1), 36–42. https://doi.org/10.1016/j.jfoodeng.2010.11.024

Bhosale, R., & Singhal, R. (2006). Process optimization for the synthesis of octenyl succinyl derivative of waxy corn and amaranth starches. *Carbohydrate Polymers, 66*(4), 521–527. https://doi.org/10.1016/j.carbpol.2006.04.007

Boroushaki, M. T., Mollazadeh, H., & Afshari, A. R. (2016). Pomegranate seed oil: A comprehensive review on its therapeutic effects. *International Journal of Pharmaceutical Sciences and Research, 7*(2), 430–442. https://doi.org/10.13040/IJPSR.0975-8232.7(2

Bustamante, A., Hinojosa, A., Robert, P., & Escalona, V. (2017). Extraction and microencapsulation of bioactive compounds from pomegranate (*Punica granatum* var. Wonderful) residues. *International Journal of Food Science and Technology, 52*(6), 1452–1462. https://doi.org/10.1111/ijfs.13422

Cao, Y., Wang, L., He, M., Zhang, Y., & Wang, H. (2014). Nanodispersions of monoglycerides of punicic acid: A potential nutrient precursor with higher oxidative stability and cytotoxicity. *RSC Advances, 4*(82), 43392–43398. https://doi.org/10.1039/C4RA06293K

Comunian, T. A., da Silva Anthero, A. G., Bezerra, E. O., Moraes, I. C. F., & Hubinger, M. D. (2020a). Encapsulation of pomegranate seed oil by emulsification followed by spray drying: Evaluation of different biopolymers and their effect on particle properties. *Food and Bioprocess Technology, 13*(1), 53–66. https://doi.org/10.1007/s11947-019-02380-1

Comunian, T. A., Roschel, G. G., da Silva Anthero, A. G., de Castro, I. A., & Hubinger, M. D. (2020b). Influence of heated, unheated whey protein isolate and its combination with modified starch on improvement of encapsulated pomegranate seed oil oxidative stability. *Food Chemistry*, 126995. https://doi.org/10.1016/j.foodchem.2020.126995

Costa, A. M., Moretti, L. K., Simões, G., Silva, K. A., Calado, V., Tonon, R. V., & Torres, A. G. (2020). Microencapsulation of pomegranate (*Punica granatum* L.) seed oil by complex coacervation: Development of a potential functional ingredient for food application. *Lebensmittel-Wissenschaft und -Technologie- Food Science and Technology, 131*, 109519. https://doi.org/10.1016/j.lwt.2020.109519

Dima, C., Pătraşcu, L., Cantaragiu, A., Alexe, P., & Dima, Ş. (2016). The kinetics of the swelling process and the release mechanisms of *Coriandrum sativum* L. essential oil from chitosan/alginate/inulin microcapsules. *Food Chemistry, 195*, 39–48. https://doi.org/10.1016/j.foodchem.2015.05.044

Flourié, B., Molis, C., Achour, L., Dupas, H., Hatat, C., & Rambaud, J. C. (1993). Fate of β-cyclodextrin in the human intestine. *Journal of Nutrition, 123*(4), 676–680. https://doi.org/10.1093/jn/123.4.676

Gangurde, A. B., Ali, M. T., Pawar, J. N., & Amin, P. D. (2017). Encapsulation of vitamin E acetate to convert oil to powder microcapsule using different starch derivatives. *Journal of Pharmaceutical Investigation, 47*(6), 559–574. https://doi.org/10.1007/s40005-016-0287-3

Gonzalez-Soto, R. A., de la Vega, B., García-Suarez, F. J., Agama-Acevedo, E., & Bello-Pérez, L. A. (2011). Preparation of spherical aggregates of taro starch granules. *Lebensmittel-Wissenschaft und -Technologie- Food Science and Technology, 44*(10), 2064–2069. https://doi.org/10.1016/j.lwt.2011.06.018

Goula, A. M., & Adamopoulos, K. G. (2012). A method for pomegranate seed application in food industries: Seed oil encapsulation. *Food and Bioproducts Processing, 90*(4), 639–652. https://doi.org/10.1016/j.fbp.2012.06.001

Goula, A. M., & Lazarides, H. N. (2015). Integrated processes can turn industrial food waste into valuable food by-products and/or ingredients: The cases of olive mill and pomegranate wastes. *Journal of Food Engineering, 167*, 45–50. https://doi.org/10.1016/j.jfoodeng.2015.01.003

Gu, F., Li, B. Z., Xia, H., Adhikari, B., & Gao, Q. (2015). Preparation of starch nanospheres through hydrophobic modification followed by initial water dialysis. *Carbohydrate Polymers, 115*, 605–612. https://doi.org/10.1016/j.carbpol.2014.08.102

Gupta, S. S., Ghosh, S., Maiti, P., & Ghosh, M. (2012). Microencapsulation of conjugated linolenic acid-rich pomegranate seed oil by an emulsion method. *Food Science and Technology International, 18*(6), 549–558. https://doi.org/10.1177/1082013211433078

Han, J. A., & BeMiller, J. N. (2007). Preparation and physical characteristics of slowly digesting modified food starches. *Carbohydrate Polymers, 67*(3), 366–374. https://doi.org/10.1016/j.carbpol.2006.06.011

He, H., Hong, Y., Gu, Z., Liu, G., Cheng, L., & Li, Z. (2016). Improved stability and controlled release of CLA with spray-dried microcapsules of OSA-modified starch and xanthan gum. *Carbohydrate Polymers, 147*, 243–250. https://doi.org/10.1016/j.carbpol.2016.03.078

Hoyos-Leyva, J., Bello-Pérez, L. A., Agama-Acevedo, E., & Alvarez-Ramirez, J. (2018a). Potential of taro starch spherical aggregates as wall material for spray drying microencapsulation: Functional, physical and thermal properties. *International Journal of Biological Macromolecules, 120*, 237–244. https://doi.org/10.1016/j.ijbiomac.2018.08.093

Hoyos-Leyva, J. D., Bello-Perez, L. A., Agama-Acevedo, J. E., Alvarez-Ramirez, J., & Jaramillo-Echeverry, L. M. (2019). Characterization of spray drying microencapsulation of almond oil into taro starch spherical aggregates. *Lebensmittel-Wissenschaft und -Technologie- Food Science and Technology, 101*, 526–533. https://doi.org/10.1016/j.lwt.2018.11.079

Hoyos-Leyva, J. D., Chavez-Salazar, A., Castellanos-Galeano, F., Bello-Perez, L. A., & Alvarez-Ramirez, J. (2018b). Physical and chemical stability of L-ascorbic acid microencapsulated into taro starch spherical aggregates by spray drying. *Food Hydrocolloids, 83*, 143–152. https://doi.org/10.1016/j.foodhyd.2018.05.002

Icyer, N. C., Toker, O. S., Karasu, S., Tornuk, F., Kahyaoglu, T., & Arici, M. (2017). Microencapsulation of fig seed oil rich in polyunsaturated fatty acids by spray drying. *Journal of Food Measurement and Characterization, 11*(1), 50–57. https://doi.org/10.1007/s11694-016-9370-8

Jiang, S., Dai, L., Qin, Y., Xiong, L., & Sun, Q. (2016). Preparation and characterization of octenyl succinic anhydride modified taro starch nanoparticles. *PloS One, 11*(2), 1–11. https://doi.org/10.1371/journal.pone.0150043

Joye, I. J., & McClements, D. J. (2014). Biopolymer-based nanoparticles and microparticles: Fabrication, characterization, and application. *Current Opinion in Colloid & Interface Science, 19*(5), 417–427. https://doi.org/10.1016/j.cocis.2014.07.002

Lawrence, P., & Brenna, J. T. (2006). Acetonitrile covalent adduct chemical ionization mass spectrometry for double bond localization in non-methylene-interrupted polyene fatty acid methyl esters. *Analytical Chemistry, 78*(4), 1312–1317. https://doi.org/10.1021/ac0516584

Melo, I. L. P. D., Carvalho, E. B. T. D., Yoshime, L. T., Sattler, J. A. G., Pavan, R. T., & Mancini-Filho, J. (2016). Characterization of constituents, quality and stability of pomegranate seed oil (*Punica granatum* L.). *Food Science and Technology, 36*(1), 132–139. https://doi.org/10.1590/1678-457X.0069

Mondragon-Jacobo, C., Hernandez-Herrera, G., & Guzman-Maldonado, S. H. (2013). Agronomical, physicochemical, and functional characterization of Mexican pomegranates as compared to Wonderful pomegranate. In *III international symposium on pomegranate and minor mediterranean fruits 1089* (pp. 299–306). https://doi.org/10.17660/ActaHortic.2015.1089.39

Phunpee, S., Ruktanonchai, U. R., Yoshii, H., Assabumrungrat, S., & Soottitantawat, A. (2017). Encapsulation of lemongrass oil with cyclodextrins by spray drying and its controlled release characteristics. *Bioscience Biotechnology & Biochemistry, 81*(4), 718–723. https://doi.org/10.1080/09168451.2016.1277942

Rincón-Aguirre, A., Bello Pérez, L. A., Mendoza, S., del Real, A., & Rodríguez García, M. E. (2018). Physicochemical studies of taro starch chemically modified by acetylation, phosphorylation, and succinylation. *Starch Staerke, 70*(3–4), 1–9. https://doi.org/10.1002/star.201700066

Sahin-Nadeem, H., & Afşin Özen, M. (2014). Physical properties and fatty acid composition of pomegranate seed oil microcapsules prepared by using starch derivatives/whey protein blends. *European Journal of Lipid Science and Technology, 116*(7), 847–856. https://doi.org/10.1002/ejlt.201300355

Shen, Z., Apriani, C., Weerakkody, R., Sanguansri, L., & Augustin, M. A. (2011). Food matrix effects on in vitro digestion of microencapsulated tuna oil powder. *Journal of Agricultural and Food Chemistry, 59*(15), 8442–8449. https://doi.org/10.1021/jf201494b

Siano, F., Straccia, M. C., Paolucci, M., Fasulo, G., Boscaino, F., & Volpe, M. G. (2016). Physico-chemical properties and fatty acid composition of pomegranate, cherry and pumpkin seed oils. *Journal of the Science of Food and Agriculture, 96*, 1730–1735. https://doi.org/10.1002/jsfa.7279

Siepmann, J., & Peppas, N. A. A. (2012). Modeling of drug release from delivery systems based on hydroxypropyl methylcellulose (HPMC). *Advanced Drug Delivery Reviews, 64*, 163–174. https://doi.org/10.1016/j.addr.2012.09.028

Singla, D., Singh, A., Dhull, S. B., Kumar, P., Malik, T., & Kumar, P. (2020). Taro starch: Isolation, morphology, modification and novel applications concern-A review. *International Journal of Biological Macromolecules, 163*, 1283. https://doi.org/10.1016/j.ijbiomac.2020.07.093, 129.

Sit, N., Misra, S., & Deka, S. C. (2013). Physicochemical, functional, textural and colour characteristics of starches isolated from four taro cultivars of North-East India. *Starch Staerke, 65*(11–12), 1011–1021. https://doi.org/10.1002/star.201300033

Sweedman, M. C., Tizzotti, M. J., Schäfer, C., & Gilbert, R. G. (2013). Structure and physicochemical properties of octenyl succinic anhydride modified starches: A review. *Carbohydrate Polymers, 92*(1), 905–920. https://doi.org/10.1016/j.carbpol.2012.09.040

Veiga, R. D. S. D., Aparecida Da Silva-Buzanello, R., Corso, M. P., & Canan, C. (2019). Essential oils microencapsulated obtained by spray drying: A review. *Journal of Essential Oil Research, 31*(6), 457–473. https://doi.org/10.1080/10412905.2019.1612788

Vernon-Carter, E. J., Alvarez-Ramirez, J., Bello-Perez, L. A., Hernandez-Jaimes, C., & Reyes, I. (2019). Role of endogenous protein in the spherical aggregation of taro starch granules upon spray-drying and in *in vitro* digestibility. *Starch Staerke*, 1900087. https://doi.org/10.1002/star.201900087

Viswanathan, A. (1999). Effect of degree of substitution of octenyl succinate starch on the emulsification activity on different oil phases. *Journal of Polymers and the Environment, 7*(4), 191–196. https://doi.org/10.1023/A:1022878631495

Yekdane, N., & Goli, S. A. H. (2019). Effect of pomegranate juice on characteristics and oxidative stability of microencapsulated pomegranate seed oil using spray drying. *Food and Bioprocess Technology, 12*(9), 1614–1625. https://doi.org/10.1007/s11947-019-02325-8